JOURNAL OF GEOPHYSICAL RESEARCH, VOL. 106, NO. D19, PAGES 22,621–22,634, OCTOBER 16, 2001

Effects of land-use modification on potential increase of convection: A numerical mesoscale study over south Israel

Nataly Perlin[1], Pinhas Alpert

Department of Geophysics and Planetary Sciences, Tel Aviv University, Tel Aviv, Israel

Abstract. The current research was designed to examine the potential of modified surface conditions in semiarid and arid central-southern Israel to enhance convective development and rainfall. The fifth-generation mesoscale model (MM5), coupled with a sophisticated land-surface submodel, is applied for the three-dimensional high resolution simulations of two convective rain case studies, on October 27, 1990 and October 18, 1987. Three surface conditions are modeled to examine the relative influence of land-use changes, which are present-time land-use (1990s), preirrigation time (1930s), and the hypothetical case of extended irrigated agricultural lands. The main conclusion of the study is that there exists a positive influence of the anthropogenic land-use changes on the enhancement of thermal convection and associated rainfall. Modification of surface parameters from semiarid land conditions to cultivated lands tends to consistently increase the potential for moist convection during the daytime heating hours, as expressed in the evolution of the PBL structure and the growth of convective available potential energy (CAPE), as well as the area-averaged rainfall. The model seems to accurately reproduce the observed atmospheric situations and rainfall, lending confidence to the assertion that these land-atmosphere effects can be quantified with an advanced mesoscale modeling system. This work is the first numerical mesobeta scale 3-D study over the south Israel area with its relatively sharp spatial change in land use as well as in climatic zone. It is believed to be a region, possibly the only in the world, where mesoscale surface and planetary boundary layer processes were suggested as causes for observed anti-desertification gains.

1. Introduction

Impact of land surface on boundary layer convective processes has been studied by numerous researchers [*Anthes*, 1984; *Collins and Avissar*, 1994; *De Ridder*, 1997, 1998; *Segal et al.*, 1988, 1989, 1995; *Segal and Arritt*, 1992]. Some authors accept that mesoscale anthropogenic climate variations may be identified, such as the desertification process followed by land overgrazing [*Otterman*, 1974; *Charney*, 1975; *Charney et al.*, 1975; *Idso*, 1980]. At the same time, the opposite process, referred to as the reversed desertification [*Alpert and Mandel*, 1986] might be expected in semiarid zones when agricultural development results in land-use changes over an extensive area.

Israel is located in the vicinity of large deserts, and its central to southern parts are classified as semi-arid and arid areas. One of the main features of such regions is the strong convective nature of rainfall, especially during the transition periods (i.e., from a dry summer to a rainy winter, or vice versa [*Sharon*, 1972; *Lockwood*, 1988]). In Israel in particular, the relatively high percentage of convective rainfall was emphasized by several researchers [*Otterman and Sharon*, 1979; *Sharon and Kutiel*, 1986]. Thus, as a rule, we deal with convective precipitation, either embedded into larger synoptic systems (as with the passage of a cold front), or induced by local circulations under favorable weather conditions.

The last few decades in Israel have been associated with intensive settlement, agricultural development, and extensive use of irrigation systems. Several indicators for possible mesoscale climate modification over central and southern Israel during this time (since the 1950s-1960s) have been reported: negative trends in diurnal wind and temperature variability [*Alpert and Eppel*, 1985; *Alpert and Mandel*, 1986], a positive trend in October rainfall amounts during the onset of the rain season, and the decrease in the spatial variability (spottiness) of rainfall [*Otterman et al.*, 1990; *Ben-Gai et al.*, 1993, 1994, 1998b].

These studies provide a basis for the hypothesis, which suggests an increase in rainfall as a result of the land surface changes [*Otterman et al.*, 1990]. The main idea is that during the fall transition period in Israel during October-November, the usual summer PBL-capping inversion weakens. Consequently, this inversion becomes more susceptible to the penetration of warm, unstable air masses inland from the Mediterranean. Under these circumstances, a slight additional surface forcing, represented by an increase in surface heat fluxes, can erode the inversion further and release the PBL potential instability, resulting in penetrating convection (above the PBL top) and the onset of rain. Upward transfer of moist air in coastal regions could also be maintained through the interaction of the midday thermal convection over land with the advancing sea breeze front [*Rao et al.*, 1999; *Wakimoto and Atkins*, 1994].

[1]Now at College of Oceanic and Atmospheric Sciences, Oregon State University, Corvallis, Oregon.

Paper number 2000JD900804.
0148-0227/01/2000JD900804$09.00

This hypothesis, however, is based mostly on climatological analysis and conceptual representation of the processes, since previous numerical studies have been limited by insufficient computing resources and lack a meteorological model that could be applied effectively to an area as small as a few tens of kilometers. Recently, *De Ridder and Gallée* [1998] explored the same case study as presented here (of October 27, 1990) with two-dimensional numerical model simulations, and they demonstrated the effect of land-surface changes on the evolution of different meteorological parameters, though without simulating rainfall. They discussed nighttime profiles of the equivalent and saturated equivalent potential temperatures for different surface conditions and deduced the increased potential for moist convection in irrigated regions. They also emphasized the necessity to further investigate the problem by utilizing a 3-D model, for a better representation of the land-atmosphere processed over a study domain. In another study by *Seth and Giorgi* [1996], it was shown that simulated surface changes produced an apparent response in precipitation, when integrated over a whole month.

The purpose of this paper is therefore to quantitatively evaluate the effects of different land-surface conditions in central-southern Israel on possible convective development and the associated rainfall, as well as to analyze convective properties of the atmosphere. It will be of primary interest to detect an expected response signal in precipitation pattern in single-day rainfall case studies. The main tool of the study is the 3-D PSU/NCAR (Pennsylvania State University/ National Center for Atmospheric Research) [*Grell et al.*, 1994] mesoscale modeling system MM5 version 2 (MM5V2), recently coupled with the land-surface PLACE (Parameterization for Land-Atmosphere Convective Exchange) model [*Wetzel and Boone*, 1995; *Perlin et al.*, 1997; *Lynn et al.*, 2001].

2. Methodology

2.1. MM5 and PLACE Models

The PSU/NCAR mesoscale modeling system MM5 [*Grell et al.*, 1994; *Dudhia*, 1993] is a limited-area model (LAM), which uses a σ-coordinate system (terrain following near the bottom) and is based on integration of the primitive hydrodynamic equations. It has fine resolution facilities, a two-way interactive nesting capability and a variety of physical options; its nonhydrostatic version is employed in the present study.

The Parameterization for Land-Atmosphere Convective Exchange (PLACE) [*Wetzel and Boone*, 1995] is designed to improve the description of land-surface processes and their feedbacks into the lower tropospheric boundary layer. The model has seven soil layers for temperature calculations and five layers for moisture exchange and storage, which are presumed to have equal hydraulic properties, depending on the soil type and soil moisture. Upper boundary conditions in PLACE are obtained from the surface energy balance, calculated by the MM5 model. Soil temperature and moisture profiles are initially set homogeneous, evolving in time in response to the atmospheric conditions.

Special attention is given to the choice of optimal model grids, as a considerable dependence of the model solution on grid resolution, grid size, and location of lateral boundaries of limited-area domains, was found by many researchers, both in weather and in climate models [*Fox-Rabinovitz and Lindzen*, 1993; *Jones et al.*, 1995; *Alpert et al.*, 1996; *Giorgi and Marinucci*, 1996]. In particular, regarding the sensitivity simulations of precipitation response to soil moisture change, considerable differences were found by *Seth and Giorgi* [1998] in regional climate models with modification of the aforementioned parameters: too coarse resolutions and too small chosen domains yielded errors in precipitation estimates. It is thus necessary to have enough resolution to adequately represent the internal forcing, while it is also desirable to have a large enough domain to include all important external lateral forcings [*Alpert et al.*, 1996].

The following two domains are chosen to meet the requirements for the present study: the coarse grid with 136 x 136 points and a horizontal grid spacing of 7.5 km, and a nested mesh with 91 x 70 points and a 2.5 km horizontal grid interval. Locations of the coarse and nested domains are shown in Figure 1a. The model has 43 vertical σ layers in both grids, stretched from the surface up to 100 hPa. There are 29 layers in the lowest 2000 m. A leapfrog scheme is used for finite differencing in time, and the time steps for the coarse and nested domains are 22.5 and 7.5 s, respectively.

The following major physical options in the MM5 modeling system are chosen: (1) the explicit moisture scheme with warm rain [*Dudhia*, 1989]; (2) MRF medium-range forecast model of the National Centers for Environmental Prediction (NCEP) planetary boundary layer scheme [*Hong and Pan*, 1996; *Troen and Mahrt*, 1986]; (3) the Kain-Fritsch sub-grid-scale cumulus parameterization [*Kain and Fritsch*, 1993] is applied on a coarse grid to include the convection triggering mechanism; nested domain uses no cumulus parameterization, and only resolved precipitation is allowed; (4) no parameterization for the radiative atmospheric cooling is used; this scheme was designed for low vertical resolution and therefore is not applied in the present study; model vertical resolution is assumed to be high enough to yield correct temperature profiles.

2.2. Land-use settings

To provide information about land-surface parameters for high-resolution numerical model experiments of the present research, a new digital land-use data set with 2.5 km grid interval is prepared for a 190 x 190 km area centered over south Israel (Figure 1b). It is based on composed albedo maps of central southern Israel for the 1990s [*Ben-Gai et al.*, 1998a], as well as a physical map of the area and vegetation maps from the Ministry of Agriculture [*Ministry of Agriculture*, 1994]. The following land types are set for the study domain (numbers relate to a category in the data set): (1) urban land, (2) plantations and irrigated crops, (3) partially irrigated crops, (4) shrubs and nonirrigated agriculture, (6) bushes and deciduous forest, (7) water, and (9) desert. Areas covered by land types 2, 3, and 4 are considered as potential areas for agriculture and are thus a subject to changes from year to year. Specific values of surface albedo, roughness length, soil wetness (ranging 0-1 from wilting point to saturation), fractional vegetation cover, and leaf area index (LAI) are assigned to each type in the following way: Albedo was assigned according to *Ben-Gai et al.* [1998a], while the values of soil wetness for our region in the season under investigation have been estimated following the consultation

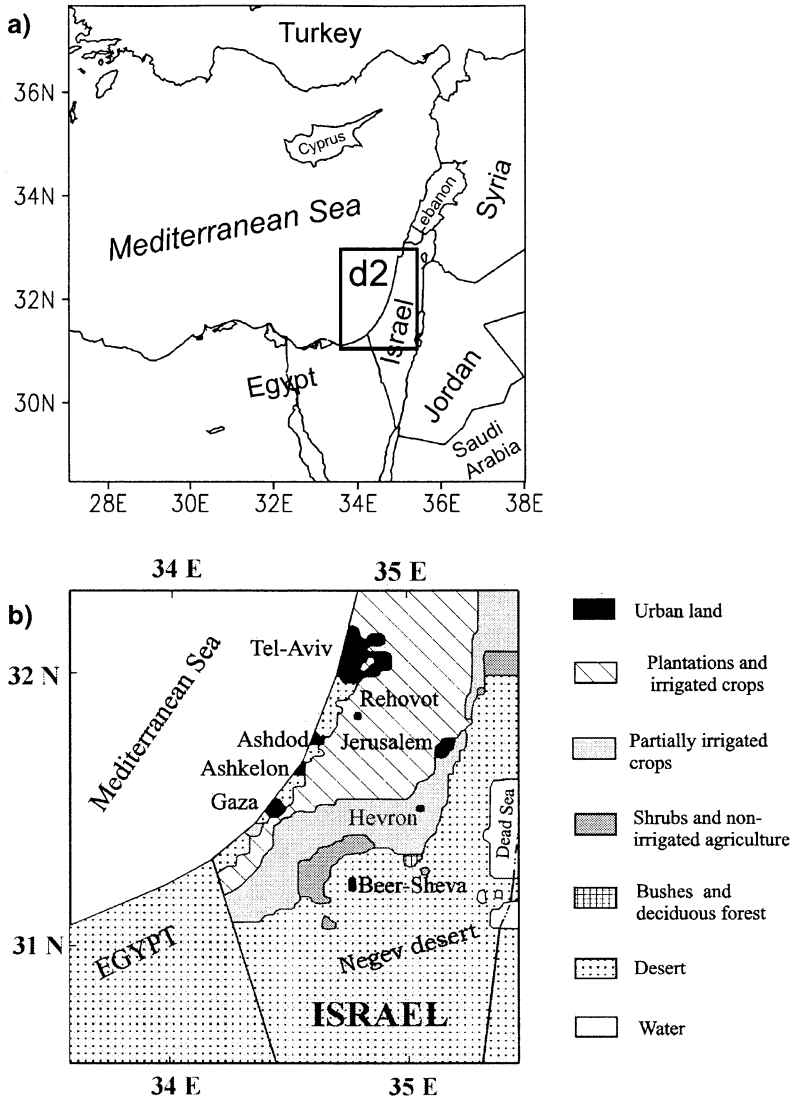

Figure 1. **(a)** Model simulations domain, where "d2" denotes the nested grid region ("domain 2"); **(b)** reconstructed land-use map of central and southern Israel corresponding to the present-time situation, i.e., the 1990s.

with Y. Mahrer (personal communication, 1998). Other parameters were estimated from the fixed land-use categories in MM5 and ISLSCP (International Satellite Land Surface Climatology Project) [*Sellers et al.*, 1992] data sets.

These parameters schematically reflect major contrasts between land types, primarily related to different agricultural development. Main features of these settings are summarized in Table 1.

The reconstructed map is smaller than the simulated domains. For the outside areas, original MM5 land-use categories with 10-min resolution are then used, which remain unchanged in all the experiments. This also requires matching the fixed land-use categories in MM5 to the ISLSCP set, to enable the PLACE model initialization.

Three surface conditions are simulated to examine the relative influence of land-use changes: (1) present time conditions (Figure 1b), (hereinafter referred to as the REAL experiment); (2) preirrigation stage (referred to as DRY), in which areas covered by plantations and irrigated crops (land type 2 in Table 1) and by partially irrigated areas (land type 3) are replaced by shrubs and nonirrigated agriculture (land type 4); this is based partially on an earlier reconstruction method of the albedo map for the 1930s [*Ben-Gai et al.*, 1998a]; (3) hypothetical "agricultural heyday" (AGRI) conditions, when land types 3 and 4 are replaced by highly developed agricultural areas (land type 2).

2.3. Boundary and Initial Data

The rain case study of October 27, 1990, was originally proposed by *Alpert et al.*, [1993] to examine the effects of surface forcing on convection and precipitation over south central Israel. Weather conditions on that day are discussed in section 3, along with the validation of model results.

Model initial and boundary conditions are produced from the NASA reanalysis data set for the Mediterranean region [*Da Silva and Alpert*, 1996], which provides meteorological fields on 18 isobaric surfaces (namely, 1000, 950, 900, 850, 800, 700, 600, 500, 400, 300, 250, 200, 150, 100, 70, 50, 30,

Table 1. Summary of the Main Parameters in the Model Land Use Set.

Data Set	Land Type Description	Albedo, %	Soil Wetness (0-1)	Rough-ness, cm	Leaf Area Index	Fractional Vegetation Cover (0-1)	Θs, $cm^3\ cm^{-3}$
1	Urban land	18.	0.05	50.	0.01	0.01	0.421
(2)	Plantations and irrigated crops	17.	0.40	20.	1.0	0.8	
(3)	Partially irrigated crops	22.	0.15	15.	0.4	0.4	0.434
(4)	Shrubs and non-irrigated areas	27.	0.07	10.	0.15	0.15	
6	Bushes and deciduous forest	16.	0.15	50.	0.8	0.6	0.434
7	Water	8.	1.00	0.01	-	-	-
9	Desert	34.	0.05	10.	0.01	0.01	0.421

Parentheses designate the types that are used or may be potentially used as irrigated agricultural lands. The parameter Θs (column 8) is the saturated volumetric moisture.

20 mb) and land surface values. The grid boxes are 2° by 2.5° in latitude and longitude, respectively. NASA reanalysis data are interpolated onto model grid points, enhanced by the local Bet-Dagan (32.00°N, 34.82°E) radiosonde observations twice daily at standard times.

Sea surface temperature (SST) is set to a constant value of 24°C, estimated for the end of October from climatological monthly means of SST for October and November in the eastern Mediterranean (in particular, along the Israeli coast; the data are from Israel Meteorological Service).

Model experiments commence at 1200 UTC (which is 1400 LT), October 26, 1990, and extend for 36 hours to 0000 UTC, October 28. Experiments are expected to simulate atmospheric conditions during the afternoon of October 27, which allows over 24 hours for model self-adjustment and spin-up. This is essential for PLACE to obtain more realistic moisture and temperature profiles in the upper soil levels following their daily evolution in response to the simulated atmospheric conditions.

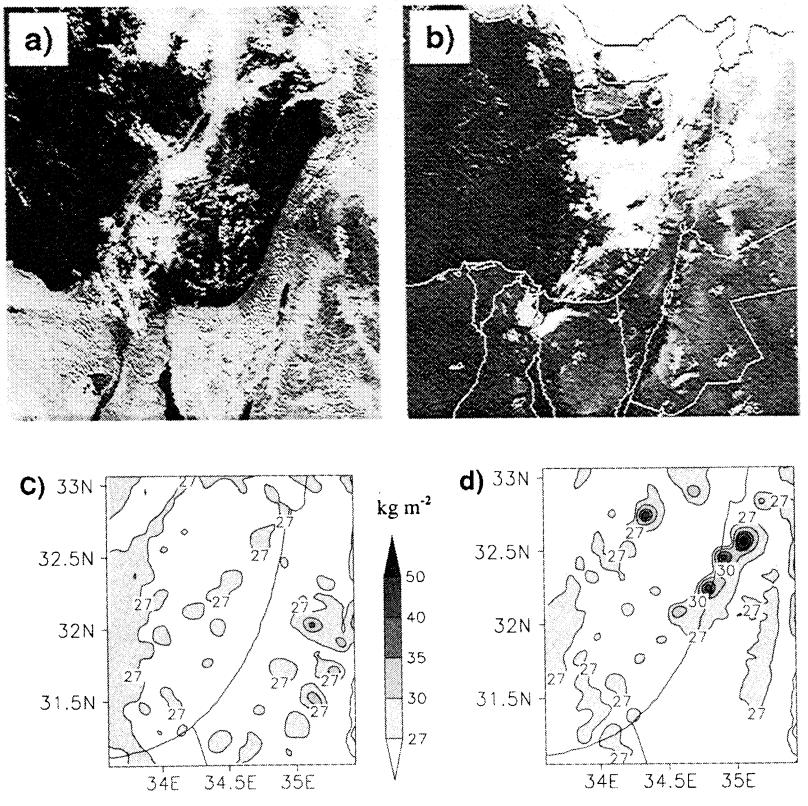

Figure 2. NOAA satellite images of the eastern Mediterranean taken on October 27, 1990, at **(a)** 1353 LT and **(b)** 1728 LT. Vertically integrated water content from REAL model simulation at **(c)** 1400 LT and **(d)** 1900 LT October 27, 1990.

3. Model Validation of October 27, 1990, Case Study

The synoptic situation on October 27, 1990, was marked by the Red Sea trough at the surface, along with a weak upper level trough to the west, a frequent synoptic condition for the fall season over the east Mediterranean. Under these conditions, low tropospheric levels are often too dry to allow rainfall. The NOAA satellite pictures (Figures 2a-2b) taken at 1353 and 1528 LT, October 27, show the progress of a frontal system over the eastern Mediterranean during the afternoon. Well-developed cloud systems appear over the Mediterranean Sea (Figure 2a), while only scattered fair weather cumulus clouds, related to a sea breeze front, concurrently appear inland over the coastal area of Egypt and Israel. A few hours later (Figure 2b), a large cloud cluster approaches the coast north of Israel, with isolated cumuli farther to the south, and at about 2000 LT rainfall of varying intensity was observed in different parts of Israel.

Figures 2c and 2d present the simulated column-integrated water content over the nested domain at 1400 and 1900 LT, respectively. Figure 2c displays scattered convective clouds inland and also indicates the cloud-free area along most of the coastline, both over sea and land, associated with the region of slight subsidence behind the progressing sea breeze front. This figure closely resembles Figure 2a, though a comparison may be difficult, as the nested domain is much smaller than the satellite picture. A plot of water content for the later time, at 1900 LT (Figure 2d), shows that the daytime convection over land terminated, and a front-like cloud chain enters Israel from the north. This is in good agreement with the satellite image in Figure 2b, which shows a large cloud cluster, penetrating the land at approximately the same location.

A precipitation map for the October 27, 1990, is given in Figure 3a, based on reports from rainstations (actual collection time is 0600 UTC of the next day). Rainfall ranges from over 30 mm in Haifa in the north, dropping steeply to ~ 5 mm in central Israel. South of Tel-Aviv, there were only a few rain centers of 2-5 mm. Accumulated rainfall for the last 24 hours of model simulation on the nested grid of the REAL experiment is presented in Figure 3b. A comparison with observed rain-gauge observations shows a fairly good agreement for a mesoscale modeling study, as both figures show high rainfall centers over north Israel (near Haifa), rapidly disappearing inland and toward the south.

Another comparison is performed between simulated vertical profiles and the radiosonde observations at the Bet-Dagan station, at 0000 UTC, October 27. The left panel of Figure 4 shows the potential temperature profiles, while the right panel is for the water vapor mixing ratio. As can be seen, the model simulates reasonably well the temperature and the shape of mixing ratio profiles, including both surface and elevated inversions.

Summarizing the model validation, the simulation reproduces atmospheric processes to an acceptable degree of accuracy, and the model can be therefore employed for the further sensitivity studies.

4. Rainfall analysis

The most important event of the simulated case was the rainfall on the afternoon of October 27, 1990. Despite the fact that rainfall is among the most difficult atmospheric parameters to predict, the current model results have shown that the simulated 24-hour accumulated precipitation field of the model run agreed well with observations. Examination of timing and intensity of the rain episodes (not shown) gives a picture of rainfall and associated convection development during the day as follows: In the morning and noon hours, thermal convection starts and enhances over land, producing

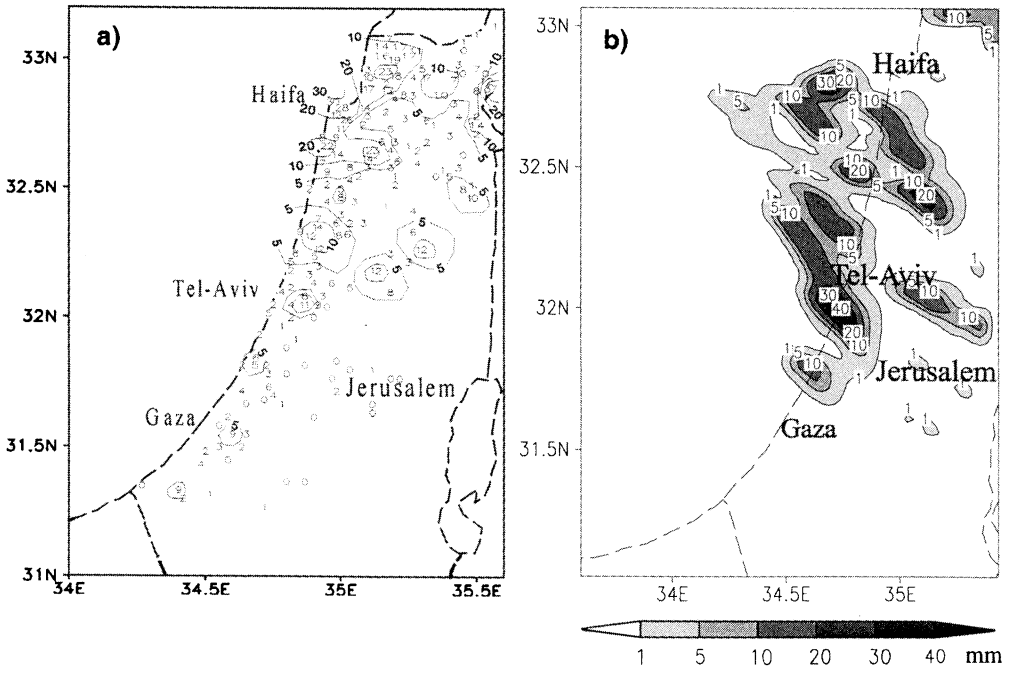

Figure 3. (**a**) Accumulated rainfall (*mm*) from over 230 rain stations on October 27, 1990. Not all stations are plotted for clarity. Contour values are 5, 10, 20, and 30 mm. (**b**) Accumulated rainfall (*mm*) in 24 hours for REAL simulation, 0000 UTC, October 27, to 0000 UTC, October 28, 1990.

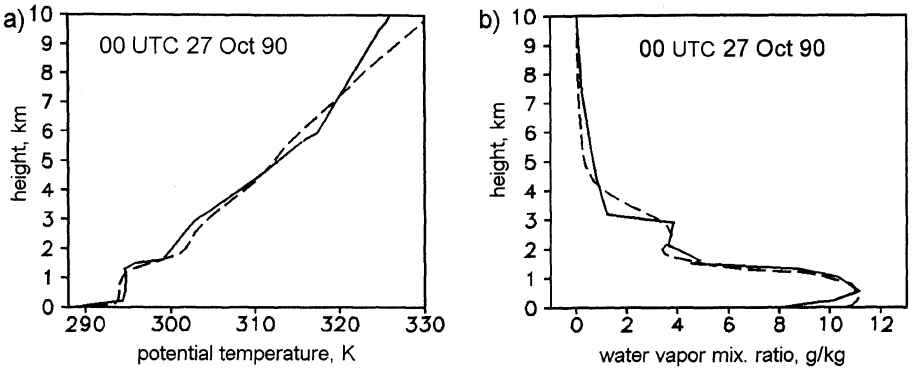

Figure 4. (**a**) Vertical profiles of potential temperature, and (**b**) water vapor mixing ratio, at the point with the coordinates 32.00°N, 34.82°E (Bet-Dagan station) at 0000 UTC, October 27, 1990, 12 hours after the simulation start. Solid lines show interpolated analysis plus radiosonde, and dashed lines denote model-resolved profiles.

patchy areas of light rain with values of tenths of millimeters to few millimeters. In the afternoon the convection over the land vanishes, and in the evening (by about 2000 LT), it becomes entirely replaced by a stronger frontal convection progressing from the northwest. Heavier precipitation is then produced over the sea and the coastal region during the evening and night.

It should be noted that in the DRY and AGRI experiments, simulated rainfall patterns are mostly similar, varying slightly in the locations of the convective cells. The major difference is the strong rain area over the mountains, produced in the REAL experiment in the late afternoon (1500 UTC, in the middle right-hand side of the picture) over the ridge of Shomron mountains (about 700 m). It can be suggested that rainfall intensifies over the mountainous region in REAL case due to the synergistic effect of increased boundary layer heights (as compared to the AGRI case) and higher moisture convergence (as compared to the DRY case).

Further analysis of the differences between cases with different land-surface conditions (e.g., DRY, REAL, AGRI cases) includes area averaging of rainfall. Averaging is performed because other methods do not seem to provide a straight correlation between the land-use changes and the resulting rainfall, which can be seen only as a combined effect on convective development and precipitation over a certain area. As, for example, the plot of the differences of 2-D rain field between two cases can only display spatial shifts of the entire rain cells.

The averaging procedure accounts for land points only (excluding water). Two areas from the nested grid chosen for averaging (Figure 5) are described: (1) Area 1, bounded by 31.05°N – 32.25°N and 34.2°E – 35.4°E, where we simulate surface parameters modification; (2) Area 2 (subregion of Area 1), which differs from Area 1 in its northern border at 31.8°N; here the contribution of the strong rain area over mountains in the REAL case is excluded. Each region is chosen to comprise as many as possible equivalent rain cells in the three simulations for consistent averaging.

For the aforementioned two regions Figure 6 presents the averaged hourly rain rates and averaged accumulated rainfall in the DRY, REAL, and AGRI experiments. These figures allow a clear separation of the daytime thermal convection and the subsequent frontal convection. The former results in rainfall starting in the morning and continuing until the afternoon (1400 UTC), followed by a short break, and then the latter frontal precipitation begins after 1700 UTC.

As can be seen, for Area 1 (Figure 6a) the rain rate for the REAL and AGRI cases consistently exceeds the DRY run at times 0900–1500 UTC. When compared, the REAL and AGRI are very close until 1200 UTC, when in the REAL experiment a strong rainfall spot appears over the mountains, resulting in a spike in the graph at 1300–1500 UTC. Averaged accumulated rainfall (Figure 6b) at 0900–1700 UTC remains lowest for the DRY run and highest for REAL. During the evening rain event, at 1900 UTC in the graph, the DRY run produced, however, the highest rain rate. For Area 2, excluding the significant rain episode over the mountains and shrinking the region of averaging (Figure 6c), results in the highest AGRI rain rates at noon and afternoon than rain rates

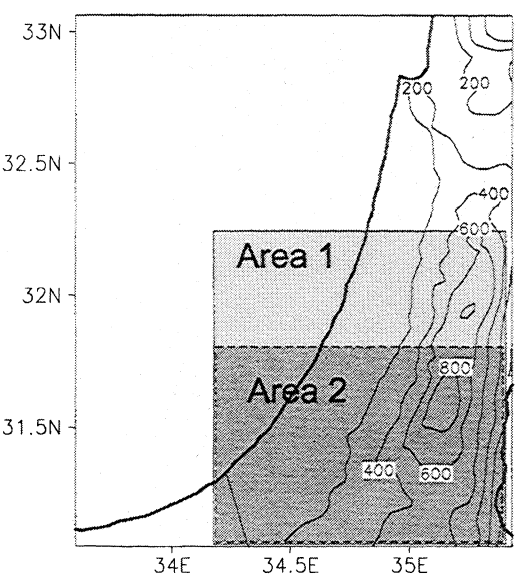

Figure 5. Areas chosen for averaging within the nested domain: **Area 1** is bounded by 31.05°N–32.25°N, 34.2°E–35.4°E; **Area 2** (part of Area 1) is bounded by 31.05°N–31.80°N, 34.2°E–35.4°E. Isolines show terrain elevation (*m*).

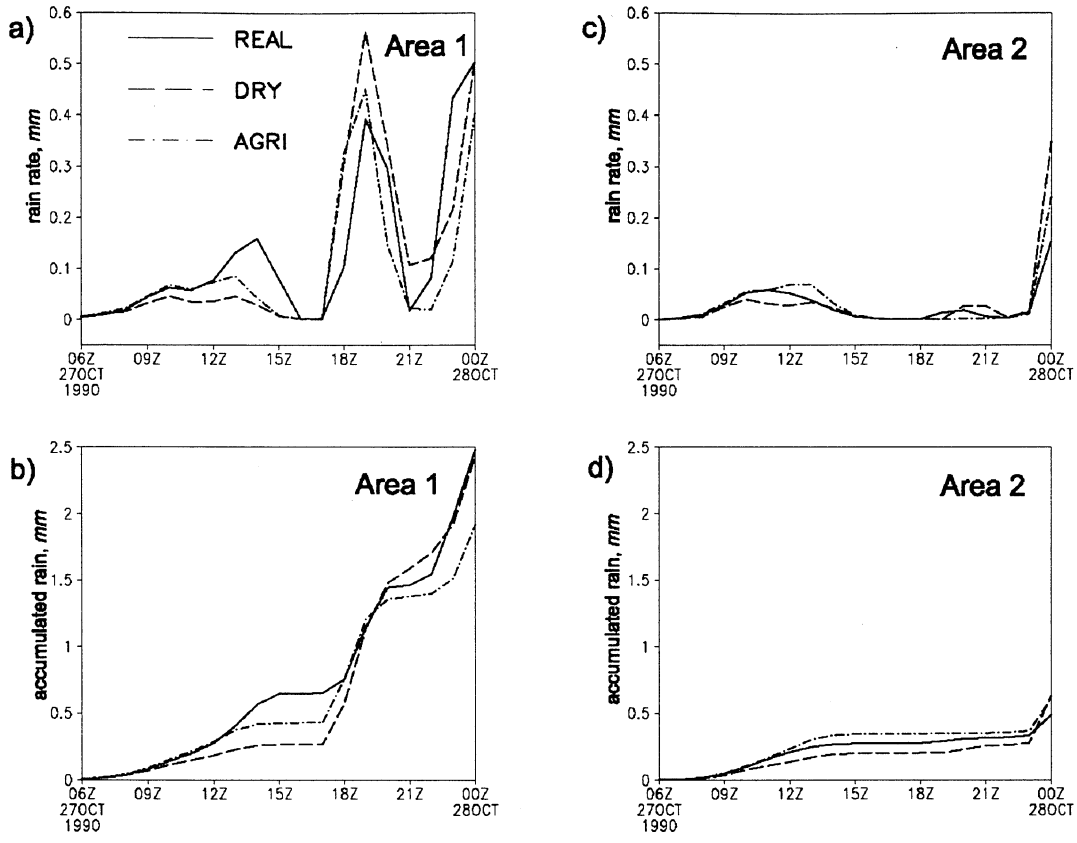

Figure 6. Hourly rain rate (top) and accumulated rainfall (bottom) averaged over land points of **(a,b)** Area 1, and **(c,d)** Area 2. Solid lines refer to REAL simulation, dashed lines DRY, and dashed-dotted lines AGRI.

in the other cases. Accumulated rainfall then remains highest for AGRI and lowest for DRY experiment at 0900–2300 UTC (Figure 6d). Table 2 summarizes Figure 6 and helps in quantitative estimation of the averaged accumulative rainfall for Area 1 and Area 2, performed for three time episodes: (1) 0600–1500 UTC, 9-hour daytime period; (2) 1500–2400 UTC, 9-hour period covering evening and night rain events; and (3) 0000 – 2400 UTC, 24-hour period. It can be seen that during noon and afternoon, the DRY case produces less rainfall, while later in the evening, higher rainfall results. During the daytime, the highest rainfall is produced by REAL (for Area 1) or AGRI (Area 2) simulations. In the October 27, 1990, experiment, frontal precipitation in the evening and night dominated over the daytime convective precipitation; by that reason, 24-hour accumulated rainfall yields higher in the DRY run. Time occurrence of the rainfall is therefore an important factor in assessment of potential rainfall increase over the study region.

Subsequent sections attempt to relate the afternoon rainfall increase patterns to the modified surface conditions (from DRY toward AGRI) and with the other changes in land-atmospheric processes.

Table 2. Accumulated Rainfall (*mm*), Averaged Over Land Points of Area 1 and Area 2, for Three Time Periods (Columns 2, 3, 4) and Three Different Surface Conditions (Column 1).

	0600-1500 UTC	1500-2400 UTC	0000-2400 UTC
		Area 1	
DRY	0.26	2.16	2.43
REAL	0.64	1.84	2.48
AGRI	0.42	1.49	1.91
		Area 2	
DRY	0.20	0.43	0.62
REAL	0.27	0.21	0.48
AGRI	0.34	0.26	0.61

5. Surface Fluxes and PBL Height

Variations in land-surface properties directly affect the surface heat budget terms, initially the surface sensible and latent heat flux are affected. At the time of maximum surface heating in the afternoon, their sum represents the daytime surface moist static energy flux, which remains unchanged as long as no modifications in land use take place. Comparisons among the three experiments of the latent, sensible heat fluxes and their sum at the surface, averaged over land points on Area 1 (from the previous section), are shown in Figures 7a-7c.

Latent heat flux is related to moisture availability and evapotranspiration at the surface, which by definition gradually increases from the DRY to AGRI case; latent heat flux is thus the highest for the AGRI experiment. Sensible heat flux is related to surface temperatures, and important conclusions can be done from further analysis. Model results show that irrigated vegetated surfaces produce lower

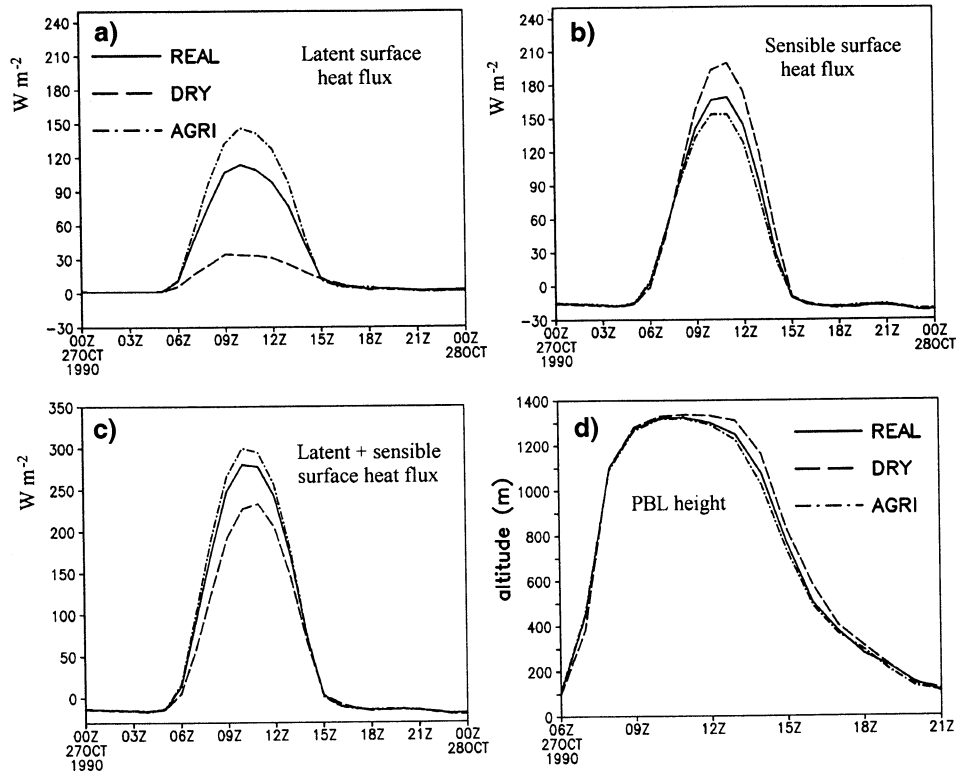

Figure 7. Diurnal cycle of **(a)** latent heat flux, **(b)** sensible heat flux, **(c)** latent plus sensible heat flux, and **(d)** PBL height, averaged over land points of Area 1. Solid lines refer to REAL simulation, dashed lines DRY, and dashed-dotted lines AGRI.

temperatures than drier areas, and sensible heat flux is highest for the DRY case. The main reason for the temperature reduction is surface cooling due to increased evapotranspiration (often mentioned as partitioning between latent and sensible heat fluxes). The sum of the surface fluxes, however, continually increases from DRY to AGRI at 0600–1400 UTC (Figure 7c). This happens because of additional factors that affect flux partitioning, as for example the lower surface albedo in the AGRI case acts to increase heat storage in the ground and yields higher surface temperatures (as suggested by *Otterman et al.* [1990]). On the other hand, the factor separation method was not employed in the present study (due to technical limitations), and it is therefore impossible to draw conclusions regarding the relative importance of other land-use parameters. All the fluxes reach their maximum values at about 1000–1100 UTC, which is nearly noon LT, at the peak of a diurnal heating cycle.

The planetary boundary layer (PBL) height calculation in the MRF PBL scheme, which was used in the simulations, is described by *Troen and Mahrt* [1986] and *Hong and Pan* [1996]. It depends on the stability condition (four different convective regimes), which are determined by the bulk Richardson number and the PBL Monin-Obukhov length. As can be seen (Figure 7d), the area averaged PBL height shows different patterns for the three cases. While it steeply increases in the morning hours in all cases, it constantly remains higher (lower) in DRY (AGRI) case during its gradual decay in the afternoon. There are no substantial differences in the PBL heights between cases during morning hours, until well-mixed boundary layer establishes in the afternoon, when information from the land surface plays an important role in PBL development. The maximal difference between AGRI and DRY occurs at 1400 UTC and exceeds 130 m. Later, after 1700 UTC, the height of the remaining residual layer varies slightly among the three cases and does not show significant differences. Note that during the daytime heating lowest PBL heights are obtained in the AGRI experiment, which at first sight do not favor the amplification of convection. It will be, however, shown later that convective development is dictated predominantly by the stability structure of the PBL and not so much by the absolute PBL height.

6. Estimation of Convective Properties of the Atmosphere

Important thermodynamic fields for the atmospheric conditions are the pseudoequivalent potential temperature θe and the saturated pseudoequivalent potential temperature θes [*Bolton*, 1980; *Holton*, 1992; *Emanuel*, 1994], which serve as indicators of convection progress.

To study differences in air parcel behavior, Figure 8 demonstrates area-averaged (over Area 1) noon profiles of the potential temperatures θ, θe , and θes at 1200 UTC from the REAL (Figure 8a), DRY, and AGRI (Figure 8b) experiments. As can be seen, in the lower troposphere, θes decreases with height up to ~1700 m. This means that this part of the atmosphere is conditionally unstable, and release of the potential instability may occur when rising air parcel reaches its level of free convection (LFC). The LFC of a non-entraining air parcel can be estimated by the method presented by *Holton* [1992]. As the air parcel is raised, it

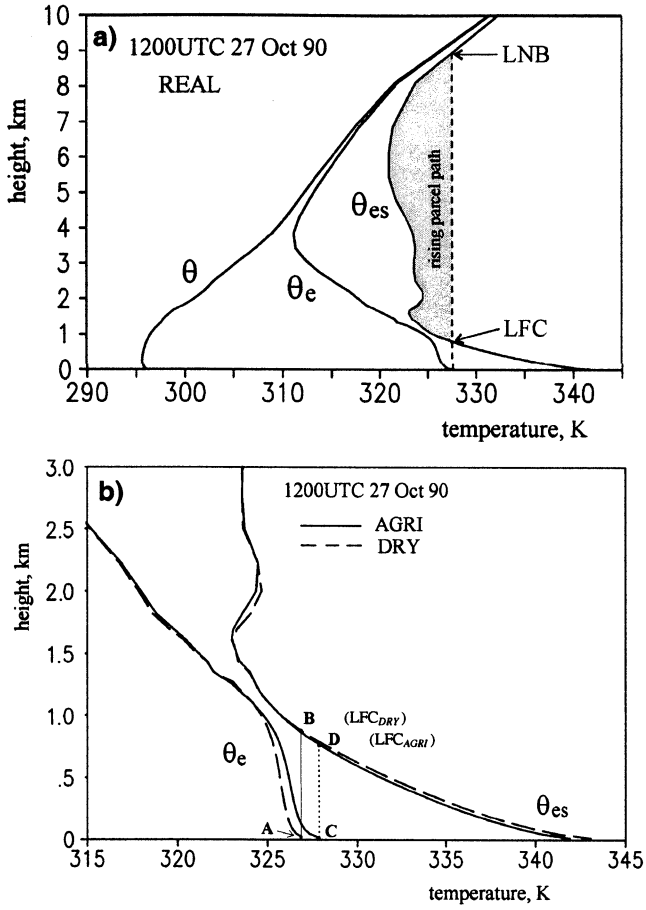

Figure 8. Averaged vertical profiles over land points of Area 1: **(a)** vertical profiles of the pseudoequivalent potential temperature (θe) and saturated pseudoequivalent potential temperature (θes) at 1200 UTC, October 27, 1990 for REAL simulation; **(b)** similar to Figure 8a, but for DRY, solid lines, and AGRI, dashed lines. See explanations in the text.

keeps its θe during the ascent from the surface (Figure 8a, the dashed vertical line upward). Comparison of this constant θe line and the θes profile of ambient air provides an estimation of parcel buoyancy at any position; the intersection point of these two lines shows the potential LFC of such a parcel. Here the term "potential" implies that the parcel must first reach saturation. Up to the LFC the parcel ascent is forced, since it has negative buoyancy. From the approximate graphical evaluation in Figure 8a, it follows that the LFC probably lies below the PBL top (compare to PBL heights in Figure 7d), and it is therefore thermal turbulent mixing inside the elevated boundary layer that serves as the lifting mechanism up to the LFC. As the air parcel reaches this level, it becomes positively buoyant and keeps ascending until the parcel reaches its level of neutral buoyancy (LNB).

Similar profiles for the DRY and AGRI cases, focused on the lower part of the atmosphere, are presented in Figure 8b. The REAL case is not shown here, as it lies between these two. The air parcel path A-B corresponds to the DRY simulation. The AGRI case produces higher θe near the surface, and thus the parcel path shifts to the right (path C-D), characterized by lower LFC. Besides the θe differences in the lower part of the PBL, LFC in the AGRI case may be also lowered by slightly cooler θes inside the boundary layer. Similarly, extending the air parcel path above the LFC would yield a level of neutral buoyancy (LNB) elevation for the AGRI. Differences in θe between the DRY and the AGRI cases at the lowest model level of 14 m above the ground is 0.9 K; the difference in θes at the same level is 1.2 K. It is worth noting that the PBL-capping inversion is well marked in the graph of θes, as an elevated inversion above 1700 m, while for the DRY case, this inversion is somewhat stronger.

Knowledge of the LFC and LNB levels is essential for the calculation of a central convective parameter, i.e., convective available potential energy (CAPE), a measure of maximum possible kinetic energy of a statically unstable air parcel, which is usually determined as integrated positive buoyancy of the rising air parcel. Similarly to *Stull* [1988], CAPE will be proportional to the area enclosed between LFC and LNB (Figure 8a, shaded). This area would expand quickly following even a small change in θes, as from DRY to AGRI in Figure 8b, which will amplify CAPE in turn. The CAPE in the AGRI experiment should therefore exceed the other cases, increasing the potential for moist convection. In addition, as the LFC point lowers, less lifting force is needed to raise air parcels to this level.

For numerical estimation of LFC, LNB, and CAPE, vertical profiles of the air virtual temperature Tv and the virtual temperature of the air parcel ascending from the lowest model level Tvp are used (not θe and θes, convenient for graphical estimation only), which are computed for each grid point of the nested grid. Table 3 shows the differences (PBL-LFC) for the time interval 1000–1500 UTC October 27, 1990, averaged over land points of Area 1, for the three cases. When this difference exceeds zero, convection is favored. As can be seen, the AGRI case first reaches this situation at 1100 UTC and remains until 1300 UTC; the REAL case favors convection only between 1200 and 1300 UTC, while the DRY experiment never reaches the positive difference. Because only averaged values are considered, the demonstrated method will work at tendencies and contrasts between the simulated surface conditions and not at absolute values. Still this can provide further evidence that small additional forcing may initiate penetrative convection.

Table 3. Differences (PBL - LFC), for Three Different Surface Conditions in the Model and for Different Times in the Afternoon.

	PBL-LFC, m		
	DRY	REAL	AGRI
1000 UTC/ 1200 LT	-416	-241	-117
1100 UTC/ 1300 LT	-146	-52	(27)
1200 UTC/ 1400 LT	-50	(19)	(53)
1300 UTC/ 1500 LT	-32	(4)	(39)
1400 UTC/ 1600 LT	-164	-59	-44
1500 UTC/ 1700 LT	-353	-247	-238

Parentheses show positive differences, which favor convection. Times are both in UTC and in LT; the first is for convenience of the comparison with other figures, while the local time relates to daylight hours.

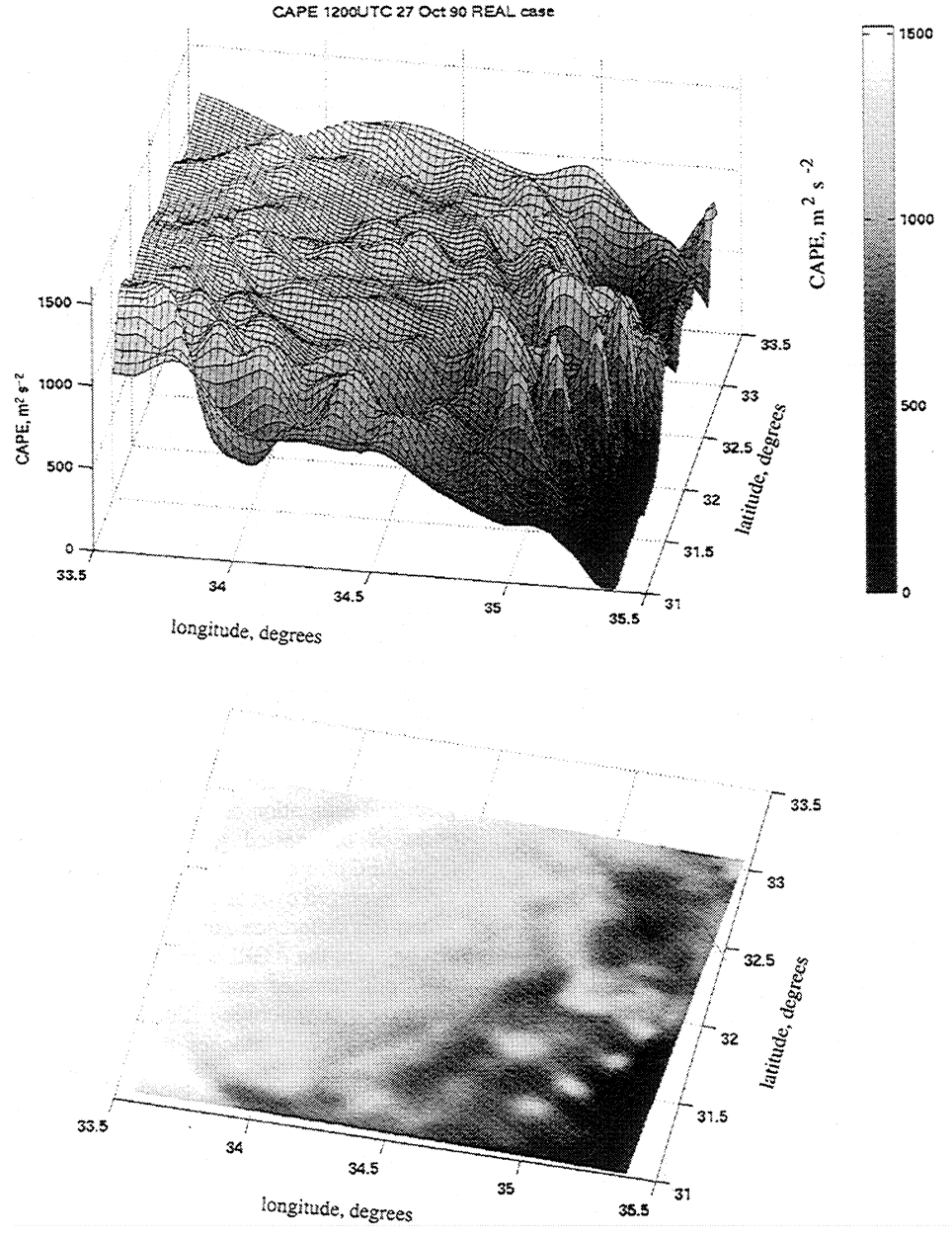

Figure 9. Calculated CAPE for the nested grid of REAL simulation at 1200 UTC, October 27, 1990: (top) a gridded 3-D plot, (bottom) its 2-D pseudocolor projection. Shading scale similar for both pictures.

CAPE estimates for an air parcel rising from the lowest model level (18 m) are calculated for the entire nested grid of the REAL simulation at 1200 UTC (Figure 9). Gray scale shading denotes CAPE values varying from zero (black) to over 1500 m^2 s^{-2} (white). Note that CAPE is high above the sea (light colors), due to the high moisture content, although convective motions are weak over water. The randomly spread low "humps" and "troughs" designate areas of slight updrafts and downdrafts, respectively. A different picture exists over the land, on the southeast quarter of the figure, where several well-defined updraft areas appear, seen as steep "hills" in the 3-D plot and as light spots in its 2-D projection, aligned parallel to the shore and mountain ridge. Eastward of the mountain ridge, steep topography gradients exist (on the east southeastern border of the domain), and where the region of strong subsidence is outlined by CAPE values close to zero (black). This figure demonstrates the high variance of CAPE across the domain, and vigorous convective updrafts alternating with adjacent downdraft regions above the heated land.

The daily evolution of the area-averaged CAPE for the three experiments (Figure 10), shows CAPE growth in the morning hours after 0600 UTC, followed by a further increase during the daytime, and then its gradual decrease in the afternoon. The CAPE is highest between 1500 and 1700 UTC. From its morning growth to 1600 UTC, the CAPE for the DRY experiment is notably lower than for the REAL and AGRI cases, consistent with the previous analyses of rainfall and fluxes. Later, after 1700 UTC the REAL experiment produces lowest CAPE. Possible reasons for this afternoon

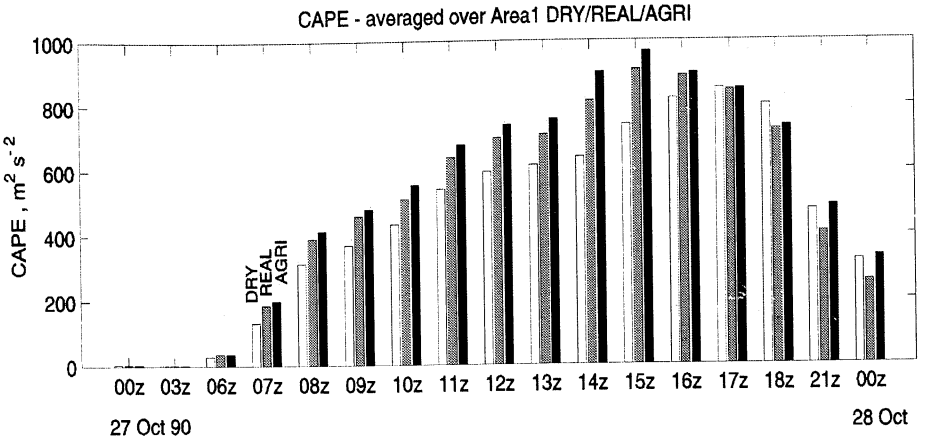

Figure 10. Daily evolution of CAPE, averaged over land points of Area 1, for the DRY (white columns), REAL (gray), and AGRI (black) simulations.

CAPE increase in DRY and AGRI simulations include the following: in the DRY case, it is the elevated PBL height, and in the AGRI case, the additional soil moisture could contribute to the atmospheric moisture. Note also that while on the night of October 27 the CAPE is nearly zero, it becomes significant (300-400 m^2 s^{-2}) on the following rainy night at 0000 UTC, October 28, in accordance with the non-stable weather on the second night over most of the region.

7. Case Study on October 18, 1987

While the case study of October 27, 1990, demonstrated the role of CAPE in increasing midday convective rainfall, the input of the case is lessened as the maximum precipitation was synoptic in nature and occurred later during nighttime hours. A second case, on October 18, 1987, is thus analyzed, in which the convective and synoptic precipitation occur simultaneously.

There are usually only a few rainfall events during October, and in some years, this month is dry. Hence the choice for numerical experiments was very limited because of preference to have cases with observed rainfall that exceeds drops in at least some of the reports but still not with heavy precipitation, which are very infrequent. Most rainfall events during this month are associated with the Red Sea trough, and this is true for the two cases chosen. These cases are therefore believed to fairly represent most of the October events. The examination of model results for the case study on October 18, 1987, is limited to the precipitation field, as it is the culminating cumulative PBL parameter, and the MM5 model was shown capable of reproducing the other thermal and dynamic fields during such an event in the previous simulations. CAPE analysis is not presented, as the same mechanisms are assumed to be valid.

For the second case study, no satellite images for the region are available, nor are reports of the rainfall timing. NASA reanalysis maps (Figure 11) used for the model initial and boundary conditions are therefore carefully examined to understand the weather conditions on this day. The synoptic situation over the eastern Mediterranean on October 17, 1987, included the Red Sea trough at the surface associated with northeasterly flow over Israel and supported by a deepening

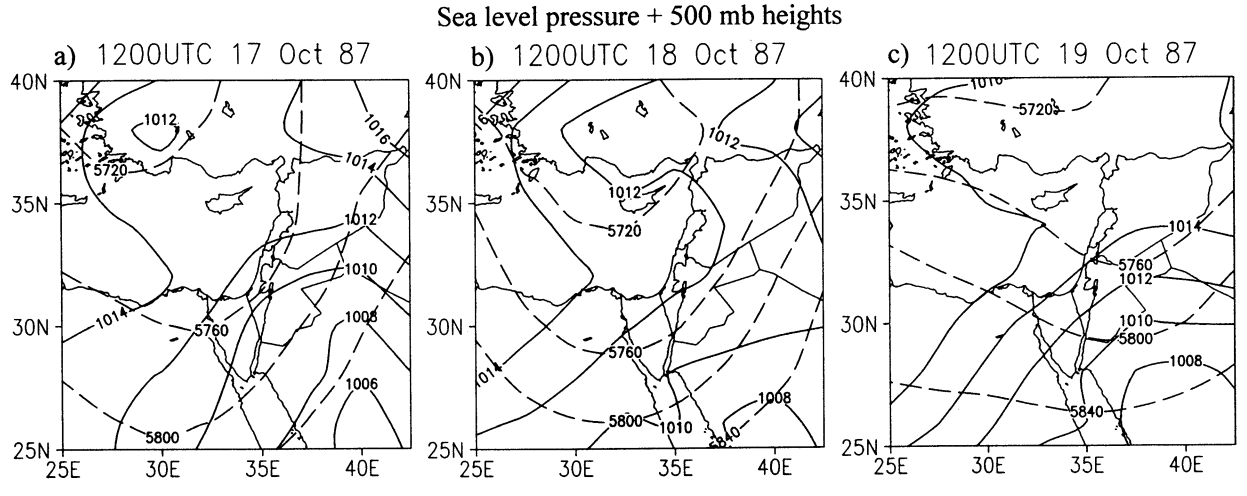

Figure 11. NASA reanalysis maps of sea level pressure (solid) and 500 mbar geopotential heights (dashed) over eastern Mediterranean at **(a)** 1200 UTC, October 17, 1987, **(b)** 1200 UTC, October 18, 1987, and **(c)** 1200 UTC, October 19, 1987.

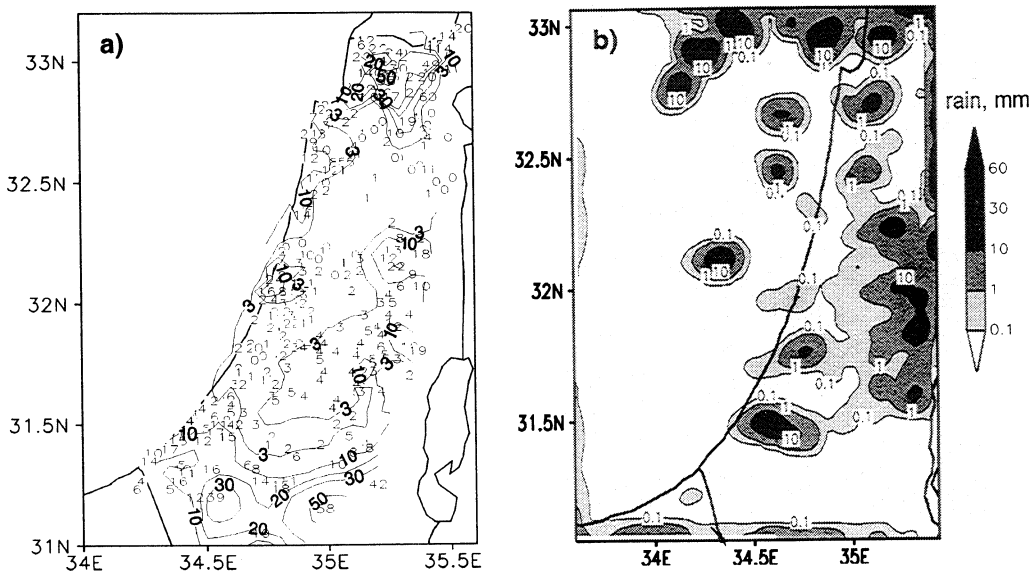

Figure 12. (a) Precipitation (*mm*) data reported from over 300 rain stations on October 18, 1987, for 0600 UTC 18 October to 0600 UTC, October 19 (not all stations are plotted). Contour values are 3, 10, 20, 30, 50 mm; (b) 24-hour accumulated rainfall in REAL2 simulation for the period 0600 UTC, October 18 to 0600 UTC, October 19, 1987.

upper air trough. By 1200 UTC, October 18, the sea level pressure pattern evolved, so moderate westerly winds determined the air transport in the lower troposphere around the Mediterranean eastern coast. By noon of the next day, October 19, when the upper air trough moved eastward, the surface Red Sea trough (with its axis to the east of Israel) was again established over the region.

Mesoscale model settings for this case study are the same to those of previous experiments (of October 27, 1990), with only two exceptions. Firstly, no radiosonde observations are used to enhance the analysis data. Secondly, the number of vertical σ levels is set to 40 (instead of 43). Model simulations start at 1200 UTC, October 17, 1987, extend 42 hours, ending at 0600 UTC, October 19, 1987. The experiments are labeled according to three different surface conditions: DRY2, REAL2, and AGRI2, where the number "2" denote the second case study.

Precipitation data from rain stations for October 18 (collecting time 0600 UTC, October 18, to 0600 UTC, October 19) in Figure 12a display patchy areas of intensive rain with 30-50 mm in centers observed both in the northern and in the southern parts of the region. The modeled 24-hour accumulated rainfall for the same period (Figure 12b) seems to be similar to the observations in the sense that rain spells appear with maxima greater than or equal to 30 mm. In the southern part of the domain, which is the northern edge of the Negev desert, the model simulates a strong rainfall center (located approximately 31.50°N, 34.65°E). These southern parts of Israel receive meaningful precipitation mostly during strong winter cyclonic systems that penetrate farther south, while in many cases, only north central Israel gets rainfall.

Rain-rate comparisons for the three simulations, DRY2, REAL2, and AGRI2, of the area averaged 3-hour rainfall and the accumulated rain (Figure 13) show that the AGRI2 (DRY2) produces more (less) precipitation during the afternoon. Rainfall partitioning among the cases at night does not seem to show a clear trend (Figure 13a), although AGRI2 still results in higher rainfall.

Hence modeling of the second case study of an October convective rain also shows a certain increase in rainfall during the daytime, which was shown in the previous sections to be related to the overall convective potential growth over the agricultural lands as compared to the dry natural vegetation. However, the second case study has an important addition to the first one, because the accumulative rainfall in the end of the simulation then follows the same tendency as during the daytime, with highest precipitation produced by AGRI2 and lowest produced by the DRY2 experiment.

8. Summary and Conclusions

The current research is designed to estimate human ability to influence rainfall development and to quantitatively evaluate the effects of different land-surface conditions in semiarid and arid central southern Israel on convection and convective precipitation. During the fall transition period, October rainfalls have been previously found to increase in recent decades, and it has been suggested that this happened because of anthropogenic land-use changes over the same area.

Simulations by the mesoscale atmospheric modeling system (MM5/PLACE) of two convective rain case studies, on October 27, 1990 and October 18, 1987, over the eastern Mediterranean region show good agreement with rain-gauge observations, including both precipitation values and timing. Three surface conditions are modeled to examine the relative influence of land-use changes: (1) present-time land use, 1990s (REAL); (2) preirrigation time, 1930s (DRY); and (3) hypothetical extensively irrigated agriculture (AGRI).

Detailed analysis of the rainfall field and associated convective properties of the atmosphere (CAPE, for example) results in the following conclusions: Modification of surface

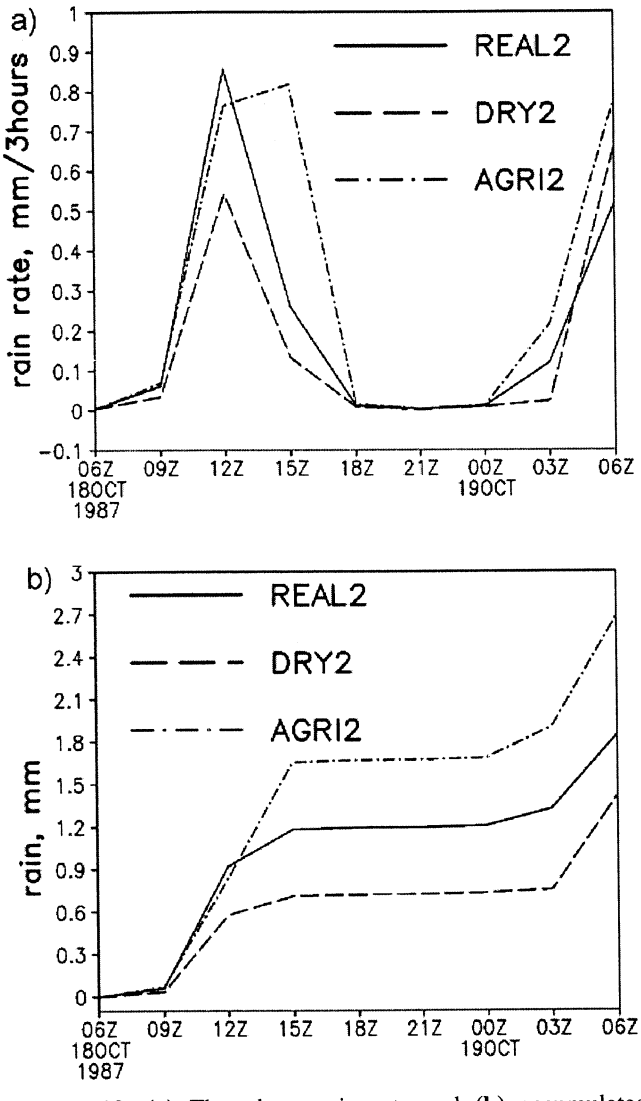

Figure 13. (**a**) Three-hour rain rate and (**b**) accumulated rainfall (*mm*) averaged over land points of Area 1 in REAL2 (solid lines), DRY2 (dashed lines), and AGRI2 (dashed-dotted lines) simulations.

parameters from semiarid land conditions to cultivated land tends to consistently increase the potential for moist convection during daytime heating hours. This, in turn, can lead to convective precipitation amplification at noon and afternoon (0800–1700 LT) under favorable weather conditions. At this time of the day, additional surface forcing may serve as a decisive factor in the initiation of penetrative convection (above the PBL top), even though the maximum effect of the surface forcing is reached at about 1400–1700 LT.

This confirms the assumption of "marginal convection" in semiarid and arid regions. If the daily precipitation maximum occurs near this time, one can therefore expect a positive atmospheric response in rainfall intensification over such arid and semiarid areas. It is worth noting here that observational studies by *Otterman and Sharon* [1979] indicated that in the continental Negev, high-intensity precipitation (implying a convective origin) had a tendency to occur in the afternoon to evening hours, while in the coastal region, a daytime dominance of broad-spectrum rain events is found for the September-November months. Also, an overall predominance of high-intensity rainfall was found in the arid Negev as compared to the more humid parts of the country [*Sharon and Kutiel*, 1986].

The main conclusion of the study is that there exists a positive influence of anthropogenic land use changes on the enhancement of thermal convection and associated rainfall, which can be quantified with an advanced mesoscale modeling system. This contributes to the original hypothesis of climate modification that has taken place over the semiarid region of Israel following the land use changes. This conclusion, however, does not exclude additional regional or global factors that may have contributed to the observed rainfall increase. Among large-scale factors is negative tendency of the mean sea level pressure or increase of the Mediterranean SST, which may lead to rainfall increase, while the "greenhouse" effect would decrease precipitation in the region.

Finally, this is the first numerical high-resolution 3-D study over the southern Israel area with its relatively sharp spatial change in land use, as well as in climatic zone. It is believed to be a region, possibly the only in the world, where mesoscale surface and PBL processes were suggested as causes for observed antidesertification gains.

Acknowledgments. This work was supported by the Israeli Ministry of Science, under contracts 1789-1-95, 1789-2-96, and 1789-3-97. Radiosonde data were provided by the Israel Meteorological Service, and we would like to thank Sarah Rubin for assistance with rain stations reports. We acknowledge Peter Wetzel and the NASA group for allowing us the use of PLACE. This study was partially supported by the US-Israel Bi-National Science Foundation grant 97-00448. Significant efforts on coupling of MM5 and PLACE model codes were done by Barry Lynn; this part of the work was supported by the USRA Visiting Scientists Program (NAS-5-32484). We acknowledge Roni Avissar, Moti Segal, and Yitzhak Mahrer for constructive discussions and useful suggestions.

References

Alpert, P., and A. Eppel, A proposed index for mesoscale activity, *J. Clim. Appl. Meteorol.*, *24*, 472-480, 1985.

Alpert, P., and M. Mandel, Wind variability – An indicator for mesoclimatic change in Israel, *J. Clim, Appl. Meteorol.*, *25*, 1568-1576, 1986.

Alpert, P., A. Manes, S. Rubin, D. O'c. Starr, J. Otterman, G. Gutman, and A. Bitan, Study of possible climatic change in Israel due to land-use modification, *BSF Sci. Rep.*, 46 pp., 1993. (Available at Dep. of Geophys. and Planet. Sci., Tel-Aviv Univ., Tel-Aviv, Israel.)

Alpert, P., S. O. Krichak, T. N. Krishnamurti, U. Stein, and M. Tsidulko, The relative roles of lateral boundaries, initial conditions and topography in mesoscale simulations of lee cyclogenesis, *J. Appl. Meteorol.*, *35*, 1091-1099, 1996.

Anthes, R.A., Enhancement of convective precipitation by mesoscale variations in vegetative covering in semiarid regions, *J. Appl. Meteorol.*, *23*, 541-554, 1984.

Ben-Gai, T., A. Bitan., A. Manes, and P. Alpert, Long-term change in October rainfall patterns in Southern Israel, *Theor. Appl. Climatol.*, *46*, 209-217, 1993.

Ben-Gai, T., A. Bitan, A. Manes, and P. Alpert, Long-term change in annual rainfall patterns in Southern Israel, *Theor. Appl. Climatol.*, *49*, 59-67, 1994.

Ben-Gai, T., A. Bitan, A. Manes, P. Alpert, and A. Israeli, Aircraft measurements of surface albedo in relation to climatic changes in southern Israel, *Theor. Appl. Climatol.*, *61*, 207-215, 1998a.

Ben-Gai, T., A. Bitan, A. Manes, P. Alpert, and S. Rubin, Spatial and temporal changes in rainfall frequency distribution patterns in Israel, *Theor. Appl. Climatol.*, *61*, 177-190, 1998b.

Bolton, D., The computation of equivalent potential temperature, *Mon. Weather Rev.*, *108*, 1046-1053, 1980.

Charney, J. G., Dynamics of deserts and droughts in the Sahel, *Q. J. R. Meteorol. Soc.*, *101*, 193-202, 1975.

Charney, J. G., P. H. Stone, and W. J. Quirk, Drought in Sahara: A biogeophysical feedback mechanism, *Science*, *187*, 434-435, 1975.

Collins, D. C., and R. Avissar, An evaluation with the Fourier Amplitude Sensitivity Test (FAST) of which land-surface parameters are of greatest importance in atmospheric modeling, *J. Clim.*, *7*, 681-703, 1994.

Da Silva, A., and P. Alpert, Documentation of the multi-year GEOS-1 assimilation data subset for the northern Africa, the Mediterranean, and the Middle East, *NASA, Data Assimil. Off. Note 96-05*, 24 pp., 1996.

De Ridder, K., Land surface processes and the potential for convective precipitation, *J. Geophys. Res.*, *102*, 30,085-30,090, 1997.

De Ridder, K., The impact of vegetation cover on Sahelian drought persistence, *Boundary-Layer Meteorol.*, *88*, 307-321, 1998.

De Ridder, K., and H. Gallée, Land surface-induced regional climate change in southern Israel, *J. Appl. Meteorol.*, *37*, 1470-1485, 1998.

Dudhia, J., Numerical study of convection observed during the winter monsoon experiment using a mesoscale two-dimensional model, *J. Atmos. Sci.*, *46*, 3077-3107, 1989.

Dudhia, J., A nonhydrostatic version of the Penn-State/NCAR mesoscale model: Validation tests and simulation of an Atlantic cyclone and cold front, *Mon. Weather Rev.*, *121*, 1493-1513, 1993.

Emanuel, K. A., *Atmospheric Convection*, 580 pp., Oxford Univ. Press, New York, 1994.

Fox-Rabinovitz, M. S., and R. S. Lindzen, Numerical experiments on consistent horizontal and vertical resolution for atmospheric models and observing systems, *Mon. Weather Rev.*, *121*, 264-71, 1993.

Giorgi, F., and M.R. Marinucci, A study of the sensitivity of simulated precipitation to model resolution and its implications for climate studies, *Mon. Weather Rev.*, *124*, 148-166, 1996.

Grell, G. A., J. Dudhia, and D. R. Stauffer, A description of the fifth-generation Penn State/NCAR mesoscale model (MM5), *NCAR Tech. Note, NCAR/TN-398+STR*, 117 pp., Natl. Cent. for Atmos. Res., Boulder, Colo., 1994 (NCAR Inf. Serv., Boulder, Colo.)

Holton, J. R., *An Introduction to Dynamic Meteorology*, 511 pp., Academic P., San Diego, Calif., 1992.

Hong, S.-Y., and H.-L. Pan, Non-local boundary layer vertical diffusion in a medium-range forecast models, *Mon. Weather Rev.*, *124*, 2322-2339, 1996.

Idso, S. B., Surface energy balance and genesis of deserts, *Arch. Meteorol. Geophys. Bioclim.*, Ser. A, *30*, 253-260, 1980.

Jones, R. G., J. M. Murphy, and M. Noguer, Simulation of climate change over Europe using a nested regional-climate model, part I, Assessment of control climate, including sensitivity to location of lateral boundaries, *Q. J. R. Meeorol. Soc.*, *121*, 1413-1449, 1995.

Kain, J. and J. M. Fritsch, Convective parameterization in mesoscale models: The Kain-Fritsch scheme, in *Representation of Cumulus Convection in Numerical Models, AMS Monogr. Ser.*, edited by K. A. Emanuel and D. J. Raymond, 165-170, Am. Meteorol. Soc., Boston, Mass.1993.

Lockwood, J.G., Climate and climatic variability in semi-arid regions at low latitudes, in *The Impact of Climatic Variations on Agriculture, vol. 2, Assessments in Semi-arid Regions,* edited by M.L. Porry, T.R. Carter, and N.T. Konijn, 85-120, 1988.

Lynn, B. H., D. R. Stauffer, P. J. Wetzel, W.-K. Tao, P. Alpert, N. Perlin, R. D. Baker, R. Munoz, A. Boone, Y. Jia, Improved simulation of Florida summer convection using the PLACE surface model and a 1.5-order turbulence parameterization coupled to the Penn State/NCAR mesoscale model, *Mon. Weather Rev., 129*, 1441-1461, 2001.

Ministry of Agriculture, *Agricultural Branches in the Years 1991-1992* (in Hebrew), 38 pp., Tel-Aviv, Israel, 1994.

Otterman, J., Baring high-albedo soils by overgrazing: A hypothesized desertification mechanism, *Science*, *186*, 531-553, 1974.

Otterman, J., and D. Sharon, Day/night partitioning of rain in an arid region – computational approaches, results for the Negev and meteorological/climatological implications, *J. Rech. Atmos.*, *13*, 11-20, 1979.

Otterman, J., A., Manes, S. Rubin, P. Alpert, and D. O'c. Starr, An increase of early rains in Southern Israel following land-use change?, *Boundary Layer Meteorol.*, *53*, 333-351, 1990.

Perlin, N., B. H. Lynn, P. J. Wetzel, and P. Alpert, A new coupling of PBLPLACE with MM5, Version 2, Results from a preliminary investigation, in *Preprints of The Seventh PSU/NCAR Mesoscale Model Users' Workshop*, Natl. Cent. for Atmos. Res., Boulder, Colo., 1997.

Rao, P. A., H. E. Fuelberg and K. K. Droegemeier, High-resolution modeling of the Cape Canaveral area land-water circulations and associated features, *Mon. Weather Rev.*, *127*, 1808-1821, 1999.

Segal, M., and R. W. Arritt, Non-classical mesoscale circulation caused by surface sensible-heat gradients, *Bull. Am. Meteorol. Soc.*, *73*, 1593-1604, 1992.

Segal, M., R. Avissar, M. C. McCumber and R. A. Pielke, Evaluation of vegetation effects on the generation and modification of mesoscale circulations, *J. Atmos. Sci.*, *45*, 2268-2292, 1988.

Segal, M., W. E. Schreiber, G. Kallos, J. R. Garratt, A. Rodi, J. Weaver, and R.A. Pielke, The impact of crop areas in Northeast Colorado on midsummer mesoscale thermal circulation, *Mon. Weather Rev.*, *117*, 809-825, 1989.

Segal, M., R.W. Arritt, C. Clark, R. Rabin, and J. M. Brown, Scaling evaluation of the effect of surface characteristics on potential for deep convection over uniform terrain, *Mon. Weather Rev.*, *123*, 383-400, 1995.

Sellers, P. J., F. G. Hall, G. Asrar, D. E. Streber, and R. E. Murphy, An overview of the First International Satellite Land Surface Climatology Project (ISLSCP) Field Experiment (FIFE), *J. Geophys. Res.*, *97*, 18,345-18,371, 1992.

Seth, A., and F. Giorgi, Three-dimensional model study of organized mesoscale circulations induced by vegetation, *J. Geophys. Res.*, *101*, 7371-7391, 1996.

Seth, A. and F. Giorgi, The effects of domain choice on summer precipitation simulation and sensitivity in a regional climate model, J. Clim., *11*, 2698-2712, 1998.

Sharon, D., The spottiness of rainfall in a desert area, *J. Hydrol.*, *17*, 161, 1972.

Sharon, D., and H. Kutiel, The distribution of rainfall intensity in Israel, its regional and seasonal variations and its climatological evaluation, *J. Climatol.*, *6*, 277-291, 1986.

Stull, R. B.: *An Introduction to Boundary Layer Meteorology*, 666 pp., Atmos. Sci. Library, Kluwer Acad., Norwell, Mass., 1988.

Troen, I., and L. Mahrt, A simple model of the atmospheric boundary layer; sensitivity to surface evaporation, *Boundary Layer Meteorol.*, *37*, 129-148, 1986.

Wakimoto, R. M., and N. T. Atkins, Observations of the sea- breeze front during CaPE, part I, Single-Doppler, satellite and cloud photogrammetry analysis, *Mon. Weather Rev.*, *122*, 1092-1114, 1994.

Wetzel, P. J., and A. Boone, A Parameterization for Land-Atmosphere-Cloud Exchange (PLACE): Documentation and testing of a detailed process model of the partly cloudy boundary layer over heterogeneous land, *J. Clim.*, *8*, 1810-1837, 1995.

N. Perlin, College of Oceanic and Atmospheric Sciences, Oregon State University, 104 Ocean Admin. Bldg., Corvallis, OR 97331-5503. (nperlin@oce.orst.edu)

P. Alpert, Dept. of Geophysics and Planetary Sciences, Tel-Aviv University, Tel-Aviv 69978 Israel. (pinhas@cyclone.tau.ac.il.)

(Received January 24, 2000; revised October 30, 2000; accepted November 14, 2000.)